Tidal mixing of estuarine and coastal waters in the Western English Channel is a control on spatial and temporal variability in seawater CO_2

Richard P. Sims[1], Michael Bedington[2], Ute Schuster[3], Andrew J. Watson[3], Vassilis Kitidis[2], Ricardo Torres[2], Helen S. Findlay[2], James R. Fishwick[2], Ian Brown[2], Thomas G. Bell[2]

[1]Department of Geography, University of Calgary, Calgary, T2N 1N4, Canada
[2]Plymouth Marine Laboratory, Plymouth, PL1 3DH, United Kingdom
[3]Department of Geography, University of Exeter, Exeter, EX4 4QE, United Kingdom

Correspondence to: Richard P. Sims (r.sims2@exeter.ac.uk) and Thomas G. Bell (tbe@pml.ac.uk)

Abstract. Surface ocean carbon dioxide (CO_2) measurements are used to compute the oceanic air–sea CO_2 flux. The CO_2 flux component from rivers and estuaries is uncertain due to the high spatial and seasonal heterogeneity of CO_2 in coastal waters. Existing high-quality CO_2 instrumentation predominantly utilise showerhead and percolating style equilibrators optimised for open ocean observations. The intervals between measurements made with such instrumentation make it difficult to resolve the fine-scale spatial variability of surface water CO_2 at timescales relevant to the high frequency variability in estuarine and coastal environments. Here we present a novel dataset with unprecedented frequency and spatial resolution transects made at the Western Channel Observatory in the south west of the UK from June to September 2016, using a fast response seawater CO_2 system. Novel observations were made along the estuarine–coastal continuum at different stages of the tide and reveal distinct spatial patterns in the surface water CO_2 fugacity (fCO_2) at different stages of the tidal cycle. Changes in salinity and fCO_2 were closely correlated at all stages of the tidal cycle and suggest that the mixing of oceanic and riverine end members partially determines the variations in fCO_2. The correlation between salinity and fCO_2 was different in Cawsand Bay, which could be due to enhanced gas exchange or to enhanced biological activity in the region. The observations demonstrate the complex dynamics determining spatial and temporal patterns of salinity and fCO_2 in the region. Spatial variations in observed surface salinity were used to validate the output of a regional high resolution hydrodynamic model. The model enables a novel estimate of the air–sea CO_2 flux in the estuarine–coastal zone. Air–sea CO_2 flux variability in the estuarine–coastal boundary region is influenced by the state of the tide because of strong CO_2 outgassing from the river plume. The observations and model output demonstrate that undersampling the complex tidal and mixing processes characteristic of estuarine and coastal environment bias quantification of air-sea CO_2 fluxes in coastal waters. The results provide a mechanism to support critical national and regional policy implementation by reducing uncertainty in carbon budgets.

1 Introduction

The ocean has taken up about a quarter of anthropogenic carbon dioxide (CO_2) emissions to date, absorbing approximately 2.5 Pg C yr^{-1} (Friedlingstein et al., 2019). Global observations of the partial pressure of CO_2 in seawater (pCO_2) are stored in the Surface Ocean CO_2 Atlas (SOCAT) (https://www.socat.info/)(Bakker et al., 2016). The latest version of SOCAT (v2021), contains ~32.7 million pCO_2 measurements, with the majority (~>75%) of data collected in the open ocean (Laruelle et al., 2018). The carbon cycle in continental shelf waters has been extensively studied in recent years (Laruelle et al., 2018;Robbins et al., 2018;Kahl et al., 2017;Ahmed and Else, 2019;Laruelle et al., 2017b;Kitidis et al., 2019;Fennel et al., 2019). Whilst the surface area of coastal, estuarine and continental shelf waters make up 7.5% of global waters (~2.7 x 10^7 km^2) (Cai, 2011), continental shelves alone have been shown to take up a substantial proportion 0.20–0.25 Pg C yr^{-1} (8-10%) of global ocean uptake (Laruelle et al., 2018;Chen et al., 2013;Cai, 2011;Bauer et al., 2013;Laruelle et al., 2014). Estuaries are net heterotrophic and thus typically oversaturated with pCO_2 with respect to the atmosphere (Laruelle et al., 2017a;Frankignoulle et al., 1998). The global air–water CO_2 flux from estuaries is thus into the atmosphere and this flux is currently perceived to roughly offset the CO_2 uptake by the continental shelves (Cai, 2011;Borges et al., 2006). However, the global estuarine air–water CO_2 flux remains highly uncertain, with estimates ranging from 0.09 to 0.78 Pg C yr^{-1} (Cai, 2011;Laruelle et al., 2010;Chen and Borges, 2009;Chen et al., 2013;Resplandy et al., 2018;Roobaert et al., 2019).

Estuaries and rivers around major ports and harbours are deep and easily accessed with large research vessels. However, many estuaries are shallow and/or have irregular topography. Navigating shallow estuaries safely, particularly at low tide, is not always possible for many ocean-going research vessels, such that mapping the *p*CO2 is challenging. The observations of *p*CO2 included in SOCAT from upper estuarine waters come from a limited number of research vessels that are typically small (~25 m long) and have shallow (~3 m) drafts. Transects of large rivers and estuaries by shallow-bottom boats identify a CO_2 concentration gradient between the mouth and source, with high pCO_2 (~10,000 ppm) upriver and pCO_2 levels similar to seawater close to the river mouth (Borges et al., 2018;Joesoef et al., 2015;Macklin et al., 2014;Bozec et al., 2012;Volta et al., 2016;Cai, 2011;Jeffrey et al., 2018b). Assessment of pCO_2 in inland waters, determined from measurements of total alkalinity (TA) and dissolved inorganic carbon (DIC), is also highly uncertain, due to limited carbonate buffering capacity at low pH, and because acids in terrestrial organic matter make an unknown contribution to the TA anions (Abril et al., 2015).

The zone where estuarine waters meet coastal waters is a physically dynamic system influenced by riverine outflow, winds, waves, and tidal cycles, hence pCO_2 is likely to vary where estuarine water and continental shelf water interact, yet there has been relatively little attention given to air–water CO_2 fluxes in this zone (Cai, 2011). Increased research effort over the past decade has shown that many processes are important in this zone (Cai et al., 2021;Ward et al., 2017;Shen et al., 2019). One holistic modelling study has tried to understand the coastal system in Eastern North America, encompassing tidal wetlands, estuaries and continental shelves (Najjar et al., 2018). The study demonstrated that, despite estuaries representing <10 % of

the domain area, interactions with shelf seas must be considered as the estuarine waters gave off more CO_2 than the shelves drew down. Eulerian studies in the estuarine zone have identified large tidal signals in pCO_2 with data collected from research vessels (Borges and Frankignoulle, 1999;Jeffrey et al., 2018a) and from moorings or fixed sites (Dai et al., 2009;Jeffrey et al., 2018a;Li et al., 2018;Bakker et al., 1996;Call et al., 2015;Ferrón et al., 2007;Santos et al., 2012). pCO_2 levels at the mouth of different rivers have been observed to co-vary with changes in river flow rate and with the tidal cycle (Ribas-Ribas et al., 2013;Canning et al., 2021;Najjar et al., 2018;Frankignoulle et al., 1996). Underway CO_2 measurements along transects have been made (Hales et al., 2005) but have not been regularly repeated through the transitional zone where estuaries connect with continental shelf waters.

Here we present weekly surface water fCO_2 observations along a <8 km transect from estuarine waters into continental shelf waters in the Western English Channel between April and September 2016 (Figure 1). The CO_2 measurement system was capable of high spatial (~0.2 km) and temporal resolution (~ 48 s) revealing substantial variations in surface fCO_2. Our aim was to examine in detail the transition zone between rivers, estuaries and the coastal zone in order to investigate variations in surface CO_2 and potential drivers of this variation. We then used the observed relationship in the CO_2 and salinity data together with the output of a high resolution hydrodynamic model of the estuary and nearshore region to estimate the spatial heterogeneity in fCO_2 and air/water CO_2 flux.

2. Study location and physical setting

This study was conducted in the English Channel off the coast of Plymouth (south-west UK) at the Western Channel Observatory (WCO, see Figure 1a), which includes the oceanographic station L4 (50.251°N, 4.221°W; (Smyth et al., 2010a) and the Penlee Point Atmospheric Observatory (PPAO, 50.319°N, 4.193°W;(Yang et al., 2019;Yang et al., 2016) among other routine monitoring activities and assets. The PPAO is a coastal land-based observatory on the Rame Head peninsula at the entrance to the Plymouth Sound. Station L4 is a coastal site ~8 km from PPAO and is a focal point of the ongoing WCO time series.

L4 is seasonally stratified between late April and early October (Smyth et al., 2010b). The onset of stratification typically drives a diatom dominated spring bloom in early April. Nitrogen limitation later in the year favours a summertime dominance of smaller plankton (Widdicombe et al., 2010). A prominent feature of the coastal region around WCO is the coastal/tidal current that entrain buoyant freshwater from the River Tamar outflow with prominent frontal features (Uncles and Torres, 2013). The River Tamar is a large source of freshwater to the region despite being a relatively small river (Uncles et al., 2015). The coastal current moves along the west coast of Plymouth Sound adjacent to the Plymouth Breakwater and toward PPAO before following the coastline towards Rame Head peninsula (Uncles et al., 2015;Siddorn et al., 2003). The River Tamar is known to be occasionally influence L4. For example salinity reductions of ~0.5 have been observed after several days of rainfall led to elevated river discharge rates (Rees et al., 2009).

The annual cycle of L4 surface water pCO_2 is mainly determined by biological activity, with the spring bloom depleting pCO_2 in April and May (Torres et al., 2020). Seawater pCO_2 increases to pre-bloom levels throughout the summer and is at equilibrium or slightly oversaturated with respect to the atmosphere in the autumn and winter (Kitidis et al., 2012;Marrec et al., 2013). Surface water pCO_2 decreases with distance offshore at all times of the year, with the greatest variability within 10 km of the coast (Kitidis et al., 2012). Changes in surface pCO_2 >40 ppm have been observed during a 24 hour eulerian study at L4 (Litt et al., 2010). Direct methane flux measurements made at the PPAO indicate that the waters around the Rame Head peninsula are influenced by the interaction between tidal cycles and the Tamar freshwater outflow (Yang et al., 2016).

3. Methods

Sampling approach:

Transects between the Breakwater in the Plymouth Sound and Station L4 were conducted weekly where possible during the study period (Figure 1b). Transects took place between 09:00 and 15:00 hrs local time using the RV *Plymouth Quest*. 15 transects were conducted on 12 non-sequential days between 10th June and 21st September 2016. RV *Plymouth Quest* takes

~40 minutes to travel directly to L4 during transects, except during a number of voyages when the ship was redirected into Cawsand Bay and/or closer to the PPAO. The underway seawater system on the ship has an intake at 3 m depth, supplying seawater for measurements of pCO_2, sea surface temperature (SST) and surface salinity (SBE45; Seabird Scientific, USA). The underway system is turned off when the ship is shore side of the Breakwater to reduce the risk of heavy biofouling and the intake of large quantities of sediment and coastal debris.

A rigid inflatable boat (*PML Explorer*) was used to sample the River Tamar on the 1st October 2014. SST and salinity were measured with a portable CTD package (SeaCat CTD 19+; SeaBird Scientific) and seawater was sampled at 9 stations along a ~25 km transect between the Breakwater and Calstock Slip (Figure 1b, 50°29.732'N, 4°12.408'W). Seawater was collected for laboratory analysis of total alkalinity (TA) and dissolved inorganic carbon (DIC) following the best practice (SOP 1 of Dickson et al. (2007)). The salinity (35.16) and pCO_2 (410.93ppm) were measured by the RV *Plymouth Quest* on the 29th September 2014 at station L4.

Seawater CO2 and carbonate system analyses:

Two independent CO_2 systems with different equilibrator designs were used to measure seawater CO_2 on the RV *Plymouth Quest*. The PML-Dartcom Live pCO_2 system (Dartcom systems Inc, UK) is permanently installed to measure ocean surface CO_2 at L4, and utilises a vented showerhead equilibrator with an equilibration time of 8 minutes (4 e-folding times). This was setup with a sampling frequency of 27 minutes (Kitidis et al., 2012). The showerhead system also measured atmospheric pCO_2 every 27 minutes. Additionally, a high-frequency and high-resolution membrane CO_2 system (Sims et al. (2017) was installed during the study period. This system utilises a membrane equilibrator (Hales et al., 2004) with a fast response time of 48 seconds (2 e-folding times) and has a high sampling frequency (1 Hz). Both CO_2 systems were calibrated with the same secondary standards (263.04 and 483.36ppm), traceable to WMO standards by cross-calibration at PML against National Oceanic and Atmospheric Administration Global Monitoring Laboratory (NOAA GML, USA) certified standards (244.91, 388.62 and 444.40 ppm). The membrane system was calibrated pre- and post-voyage (~4–5 hours apart) and the showerhead system calibrated hourly while the underway system was running.

The membrane and Dartcom systems used non-dispersive infrared gas analysers (Model 840B and 7000, respectively; Licor, Inc., USA) to measure gas phase CO_2 mixing ratio (xCO_2) in the equilibrated gas exiting the membrane or shower-head equilibrators. The fugacity of CO_2 inside the equilibrator ($fCO_{2(eq)}$) and the fugacity of CO_2 in seawater ($fCO_{2(sw)}$) were calculated using measured SST, surface salinity, equilibrator pressure and equilibrator temperature, using equations listed in SOP 5 (Dickson et al., 2007). Lag-time correlation analysis between SST and the equilibrator temperature identified that a -79 sec adjustment should be made to the fCO_2 measurement time. The fCO_2 time adjustment accounted for the time taken for water to enter the seawater intake beneath the hull of the ship and arrive at the showerhead and membrane equilibrators. The flux (F) of CO_2 (mmol m^{-2} d^{-1}) is computed following (Wanninkhof, 2014b):

$$F_{(sea\text{-}air)} = k_W\, k_0\, \Delta fCO_2\, SF \quad (1)$$

k_w is the water phase gas transfer velocity (cm hr^{-1}; Equ. 2), k_0 is the solubility of CO_2 in seawater (mol L^{-1} atm^{-1}) from Weiss (1974), ΔfCO_2 is the difference in fugacity between the atmosphere and ocean (µatm; Equ. 3), and SF is a scaling factor of 0.24 to express the result flux F in units of (mmol m^{-2} d^{-1}).

The gas transfer velocity is computed following Nightingale et al. (2000):

$$k_W = (0.222\,(U_{10})^2 + 0.333\,(U_{10}))\,(Sc/660)^{-1/2} \quad (2)$$

where U_{10n} is the mean wind speed at 10m height and for neutral conditions, Sc is the scaling by unitless Schmidt number of 660 (Wanninkhof, 2014a). U_{10n} measurements were taken from the L4 buoy (Smyth et al., 2010a).

ΔfCO_2 is here defined as the difference between the seawater interface fugacity and the fugacity of air:

$$\Delta fCO_2 = fCO2_{(sw)} - fCO_{2(air)} \quad (3)$$

To account for the cool and salty layer at the atmosphere ocean interface, -0.17°C and +0.1 were added to the in situ temperature and salinity when calculating seawater fCO_2 at the interface and for the estimation of air–sea CO_2 flux (Woolf et al., 2019).

TA samples were measured by open cell potentiometric titration with 0.1M hydrochloric acid on a Total Alkalinity Titrator (Model AS–ALK2; Apollo SciTech, Inc. USA) following SOP 3b in Dickson et al. (2007). DIC was measured using an Apollo SciTech DIC analyser (Model AS-C3; Apollo SciTech, Inc., USA) following SOP 2 in Dickson, Sabine et al. (2007), by acidifying samples with excess 10% phosphoric acid and using nitrogen gas to transfer liberated CO_2 to an infrared gas analyser (Model Licor 7000, Licor Inc., USA). These two measurement systems are described in more detail in (Kitidis et al., 2017). fCO_2 was calculated from TA and DIC using CO2SYS in Matlab (Van Heuven et al., 2011) with the carbonic acid dissociation constants of Mehrbach (1973) refit by Dickson and Millero (1987) and the hydrogen sulphate dissociation constant of Dickson (1990).

Numerical model:

The hydrodynamics of the WCO were modelled following Uncles et al. (2020) using an implementation of the Finite-Volume Community Ocean Model (FVCOM;(Chen et al., 2003)). The model domain (~ 49.7° to 50.6° N and ~ 4.8° to 3.8° W) encompasses station L4, PPAO, Plymouth Sound, and the estuary of the River Tamar including its major tributaries. FVCOM utilises an unstructured grid consisting of a mesh of variable resolution triangles, which allows the representation of complex coastlines and higher resolution in areas of interest whilst remaining computationally feasible. The resolution of the model is ~600 m at L4, becoming finer towards the PPAO and Plymouth Sound (~85 m), with highest resolution around the upper River Tamar channel (~40 m). The vertical system is terrain-following sigma coordinates with 24 equally spaced layers. Horizontal mixing is parameterised through the (Smagorinsky, 1963) scheme and vertical turbulence closure through

an updated version of the MY 2.5 scheme(Mellor and Yamada, 1982), with mixing coefficients of 0.2 and $1x10^{-5}$ respectively.

Water depth within the model domain uses the EMODNET bathymetry product with a nominal resolution of 1/16 degree. In the estuary and nearshore areas (< 20 m depth) the data have been complemented with local data sources of Lidar, single and multi-beam surveys accessed through the Coastal Channel Observatory (CCO, https://www.channelcoast.org/). The CCO data was re-projected from its original projection (OSGB) to WGS84 and concatenated and averaged into a 20 m regular grid using the Generic Mapping Tools (GMT 5.3.2) software (http://gmt.soest.hawaii.edu/). The merged dataset was processed using the ROMS toolbox for bathymetry processing downloaded from https://github.com/dcherian/tools. The scattered bathymetry was interpolated to 25 m and smoothed iteratively to achieve a Haney number less than 2 (Haney, 1991).

Lateral boundary conditions are provided as a one-way direct nesting at hourly resolution from a larger FVCOM model covering the west UK shelf (Cazenave et al., 2016). The surface atmospheric forcing is from the NCEP GFS 6 hourly historical product, which is downscaled to ~3 km resolution using a triple nested implementation of the Weather Research and Forecasting (WRF) model (Skamarock et al., 2008). The freshwater input flux for 11 rivers in the domain was obtained from daily river gauge data from the National River Flow archive (https://nrfa.ceh.ac.uk). The temperature of freshwater inputs was determined using a regression model on the WRF 2m air temperature, which was trained on temperature records from the UK Environment Agency's Freshwater River Temperature Archive (Orr et al., 2010) and data from the Westcountry river trust.

The model was run for the period between March 2016 and November 2016, with instantaneous values output hourly. Only the uppermost layer of the FVCOM output is used in the analysis below. The thickness of this layer varies between 0.05 m and 5m across the domain (because the model uses terrain-following coordinates), and the significance of this and how it relates to the 3 m underway measurement and air–sea CO_2 fluxes is discussed below.

4. Results

Showerhead vs membrane comparison:

Surface fCO_2 was measured for several hours while RV *Plymouth Quest* was stationary at L4 in between outbound and return transects. The showerhead system sampled continuously from the fixed seawater intake (3 m depth). The membrane equilibrator system was switched to sample via tubing from a near surface ocean profiler (Sims et al., 2017) when at L4 (Figure S1). The two CO_2 systems showed good agreement when the surface ocean profiler was between 2.5m and 3.5m, despite sampling slightly different water through different tubing (Figure 2). The mean residual was 2.77 µatm and the RMSE was 6.9 µatm when sampling on station (Figure 2), this is similar to the ±2 µatm difference that has been observed

during other seawater CO_2 intercomparison exercises (Körtzinger et al., 2000;Ribas-Ribas et al., 2014;Jiang et al., 2008). The CO_2 systems both sampled from the underway seawater supply of the ship during the L4 to Breakwater transects, and fCO_2 was estimated from pCO_2 using the underway SST and salinity. The 11 coincident fCO_2 measurements during the transects had a mean residual of 2.88 µatm and a RMSE of 27.1 µatm (Figure 2). The largest differences between the CO_2 systems tend to occur when the ship was not on station at L4.

Spatial and temporal variation in salinity, SST and fCO_2:

Sea surface salinity at L4 during the June to October study period does show small variation (mean ±SD = 35.15±0.08; Figure 3a). The L4 salinity range during the study period is within the range of previous years (Smyth et al., 2010b). L4 salinity decreased intermittently, with a maximum reduction of 0.68 on 9th August. The salinity measurements at L4 contrast with the large variability in Breakwater salinity during the study period (34.17–35.23). The average salinity difference between the Breakwater and L4 is 0.36. The salinity ranges observed at L4 and at the Breakwater are similar to model results during a tidal cycle (Uncles et al., 2015).

Coastal SSTs (Figure 3b) followed the seasonal warming pattern slowly increasing from 13.9°C on 10th June to 16.7°C on 21st September. The warming trend was in broad agreement with SST trends observed during previous years (Smyth et al., 2010b). The SST variation along each transect was typically small (<1°C) compared to the SST change over the study period (2.8°C). The smallest temperature difference between L4 and the Breakwater (0.025°C) occurred on 15th September. The largest temperature differences occurred during early summer (1.20°C, 0.63°C, 0.59°C and 0.65°C on 10th, 15th, 22nd and 30th June, respectively).

L4 surface fCO_2 increased from 355 µatm to 420 µatm between 10th June and 21st September (Figure 3c). The average fCO_2 difference between L4 and the Breakwater was 20 µatm. Abrupt changes in fCO_2 were observed along the transects, generally close to the Breakwater (>4 km from the L4 station). fCO_2 in waters within 4 km of the Breakwater ranged between 338 and 440 µatm during the study period. fCO_2 measurements within 2 km of the PPAO also varied considerably during some of the transects; for example, fCO_2 varied between 337 and 434 µatm during the transect past the PPAO on 7th July. The variability in membrane equilibrator fCO_2 measurements agreed with previous observations in the region (Kitidis et al., 2012).

When transects were ordered by stage along the 12 hour tidal cycle, the spatial variability in salinity transects (Figure S2) appeared to correspond to the different stages of the tidal cycle. Temperature and fCO_2 transects can be found in the supplementary materials (Figure S3-4). We divided our transect data according to the stage in the tidal cycle (determined from the Devonport tidal gauge station; 50.368°N, -4.185°W, Figure 1b). Transects were characterised by the time elapsed since the last period of low water (i.e. LW + X hrs) using the time at the midpoint of each transect.

Four categories were used, corresponding to 3 hr tidal periods: Low water (LW+0 hrs); Flooding tide (LW+3 hrs); High water (LW+6 hrs); and Ebbing tide (LW+9 hrs). Four transects are used below to exemplify the relationship between the different stages of the tidal cycle and the spatial variation in fCO_2 (Figures 4–7).

Example transects:

The transect on 7th July (low water, LW+0 hrs) began at L4 and headed inland (Figure 4). Salinity was 35.1 close to L4 and declined along the transect. The low salinity was directly North of PPAO (34.7), and in the shallow waters of Cawsand Bay (North of PPAO, 35.5). SST was warmest near L4 and in the relatively shallow Cawsand Bay. The river water was cooler than the L4 seawater and there was a negative gradient (0.55°C) into Cawsand Bay. fCO_2 was lowest (~360 µatm) when near to L4 and highest (~430 µatm) immediately South of PPAO. fCO_2 to the North of PPAO in Cawsand Bay was ~390 µatm, lower than waters South of PPAO.

The data collected on 15th June is an example from a flooding tide transect (LW+3 hrs, Figure 5). Salinity was 35.1 in waters close to L4 and decreased toward PPAO and the Breakwater (34.7 minimum). The Tamar river plume was warmer than coastal waters in July. SST was highest (~14.1°C) close to the Breakwater and the coldest water along the transect (13.3°C) was near to L4. The difference in fCO_2 between L4 and the Breakwater was ~18 µatm, with higher fCO_2 (353 µatm) in the warm, low salinity water close to the Breakwater.

Data collected on 30th June is an example of a transect at high water (LW+6 hrs, Figure 6). High salinity (>35) water was observed much closer to PPAO during the LW+6 hr transect than on transects during low water periods in the tidal cycle (Figures 4&5). Salinity reduces rapidly to 34.1 in between the PPAO and the Breakwater. Spatial patterns similar to surface salinity are seen in SST and fCO_2, with the gradients the inverse of the salinity gradient. The low salinity water close to the Breakwater has higher SST and fCO_2 (14.8°C and 385 µatm) than the observations South of PPAO. The fCO_2 range on this transect was ~38 µatm, and the majority of the change was close to the PPAO. The fCO_2 difference between L4 and the water just South of PPAO was only ~12 µatm. These data suggest that the Tamar plume during LW+6 hrs was restricted near to the coast and did not make a big impact upon the waters in between PPAO and L4.

Data on 10th June show a transect during an ebbing tide (LW+9 hrs) (Figure 7). Salinity near to L4 was 35.15 and declined toward the coast, interrupted by a patch of water due east of PPAO with salinity levels similar to L4. Two patches of low salinity water (34.8) were encountered along the transect. One low salinity patch was just South of PPAO and the other patch was close to the Breakwater. Spatial variation in SST and fCO_2 coincide with the variations in salinity, with higher SST (~14.2°C) and fCO_2 (~365 µatm) in the patches of low salinity water. The fCO_2 difference between L4 surface waters and the fresh, warm waters influenced by the River Tamar plume is ~25 µatm.

In summary: The variations in salinity observed in all transects (i.e. examples above and those in Supplementary Figure S2) qualitatively agreed with output from a previous physical model of the Plymouth Sound (Siddorn et al., 2003). The freshwater plume at low water extends out past the PPAO, whereas the plume at high water (LW+6 hrs) is restricted to close to the breakwater (Siddorn et al., 2003). The same model on an ebbing tide predicts that two plumes of river water exit via the channels at the east and west ends of the Breakwater.

Relationship between salinity and fCO_2:

The changes in salinity and fCO_2 during the example transects suggest that the changes in fCO_2 are driven by conservative mixing of salt and fresh water end members. Robust fCO_2 and salinity relationships have been observed in large river plumes like the Amazon and Mississippi (Lefèvre et al., 2010;Cai et al., 2013). The relationship between salinity and fCO_2 is complicated by the seasonal variability in fCO_2 and the constantly changing position of the tidally-controlled freshwater plume. We calculated the difference between *in situ* data from transects and from measurements at L4 to account for seasonal variations in seawater CO_2:

$$\xi fCO_2 = \text{Transect}_{fCO2} - \text{L4}_{fCO2} \quad (4)$$

$$\xi S = \text{Transect}_{\text{Salinity}} - \text{L4}_{\text{Salinity}} \quad (5)$$

ξfCO_2 and ξS displayed an apparent relationship throughout different seasons and stages of the tidal cycle (Figure 8). ξS was a stronger predictor of ξfCO_2 than location along the transect (distance from L4).

The fCO_2 and salinity data diverged from the general trend when the RV *Plymouth Quest* travelled into Cawsand Bay (West of the Breakwater) on 7th July (Figure 8). Uncles and Torres (2013) showed that the seawater residence time increases as you approach the Breakwater, following that methodology the FVCOM model used here also shows this is true for Cawsand Bay. A long residence time and a shallow water column mean that the waters in Cawsand Bay are likely to be closer to equilibrium with the atmosphere due to relatively higher turbulent mixing from bottom stress and surface waves (Upstill-Goddard, 2006). As Cawsand Bay is a microscale environment ($<1km^2$), the bay could be a biological hotspot driving the changes in CO_2. Excluding the 7th July transect that went into Cawsand Bay, the linear fit to the ξfCO_2 and ξS data gives $\xi fCO_2 = -39.83\ \xi S + 5.50$ (R^2=0.2165, N=22262, p=<0.001). The fit explained 21.6% of the variability in the data, with a RMSE of 18.95 μatm.

fCO_2 calculated from TA and DIC bottle data from the River Tamar on 1st October 2014 show a qualitatively similar relationship between salinity and fCO_2 (Figure S5) for stations T3–T9. The trend continues for stations furthest upstream (T1 and T2), but does not follow the same linear relationship. A linear fit between ξS and ξfCO_2 for stations T3–T9 suggests a 42.24 μatm change per unit of salinity. The bottle data indicates that the ξfCO_2 and ξS relationship can be extrapolated to lower salinities and that the relationship begins to break down at $\xi S < -4$. Note that the TA/DIC data and fCO_2 data were

collected at different times (years and stages of seasonal cycle) and with different sampling and analytical approaches. The apparent linear relationship between $\xi fCO_2$and ξS suggested that it can be applied to the wider coastal region. The next section assesses the utility of the high resolution model (Uncles et al., 2020) to predict coastal fCO_2.

Using FVCOM to estimate coastal air–sea CO_2 fluxes:

Extrapolation of the relationship between ξS and ξfCO_2 across the coastal domain required that FVCOM accurately replicates available surface salinity observations at different stages of the tidal cycle. FVCOM compares very well with the spatial and temporal variability in the four example transects at different stages of the tidal cycle (Figure 9), even though the hourly resolution of the model means the model output frequency can not capture subtle changes in frontal positions that are penalised in point-to-point comparisons. Model agreement with the ξS observations ($-0.1 > \xi S < 4$) from all 15 transects was also good (RMSE=0.213), which indicates that FVCOM can be used as a reliable indication of spatial and temporal salinity changes during the observation period (June–September 2016) (Figure S6).

Modelled spatial variations in coastal surface salinity are shown in Figure 10a, which focuses on the 7th July transect. Equivalent plots for the other three example transects on 30th June, 15th June and 10th June (Figures S7 to 9). The 7th July transect was at low water (LW +0 hrs), and when low salinity water was exiting from either side of the Breakwater and wrapping around the Rame Head Peninsula (Figure 10a).

FVCOM output was combined with surface measurements of fCO_2 at L4 (Kitidis et al., 2012) to predict coastal variability in air–sea CO_2 fluxes (Figure 10b). The model domain for estimated fCO_2 is restricted i) to cover the region inshore of L4 (>50.24°N, Figure 10b), ii) to avoid regions where gas exchange is largely caused by bottom driven turbulence (bottom depth >10 m), and iii) to avoid over-extrapolating the relationship observed in Fig 8 ($\xi S > -4$, equivalent to a minimum salinity of approximately 30). The model domain excludes the upper sections of the rivers, and the upper estuary and shallow coastal waters such as Cawsand Bay. The model results suggest that the majority of the coastal waters (Plymouth Sound and surroundings) contain fCO_2 levels that are substantially higher (>100 μatm) than L4 at this stage of the tidal cycle (low water, LW+0 hrs).

The standard combined uncertainty for calculated fCO_2 values is consistent with the International Bureau of Weights and Measures (BIPM) Guide to the expression of uncertainty in measurement (GUM) methodology (JCGM, 2008). In determining ξS, there is the uncertainty in modelled salinity (Transect $_{Salinity}$) given as the RMSE of the model salinity (0.213) and the instrument uncertainty in the salinity at L4 (L4 $_{Salinity}$ for Wetlabs WQM = 0.003; (Smyth et al., 2010a)), which add in quadrature. The combined model and instrument ξS uncertainty is propagated through the $\xi fCO2$ and ξS equation to give an uncertainty due to ξS (8.48 μatm). The standard combined uncertainty in fCO_2 includes the uncertainty in the ξfCO_2 and ξS relationship (18.95 μatm), uncertainty due to ξS (8.48 μatm) and the uncertainty in the fCO_2 observations

(L4 fCO_2 = 6.9 µatm, from the on station comparison, Figure 2). These uncertainties add in quadrature to give a standard combined uncertainty of 21.88 µatm.

The FVCOM model enables simulation of a full tidal cycle so that the impact on air–sea CO_2 flux can be visualised throughout 7th July (Figure 11, equivalent figures for the examples on 30th June, 15th June and 10th June are in Figures S10 to S12). A constant wind speed (equal to the mean during that period) is applied across the model domain (surface area = 132 km^2) for simplicity. The flux signal co-varies with tidal height (Figure 11a-b). The flux integrated across the model domain changes substantially throughout the tidal cycle (~9% change). If the region is restricted further to include just the area north of PPAO (>50.32°N) then the magnitude of the flux changes substantially from a weak sink (~-65 mol hr^{-1}) at low tide to a substantially larger sink (~-1100 mol hr^{-1}) at high tide.

Three configurations were used to calculate the flux (Figure 12) to establish whether the tidal plume had a net effect on the regional air–sea fluxes calculated on seasonal timescales between March and November 2016. In the first configuration (L4), L4 measurements were extrapolated across the study area. The second configuration (this study) combined the L4 measurements with the fCO_2 and salinity relationship (Figure 8), and applied the result to the spatially varying salinity field from the FVCOM model. In the third configuration (Landschützer coastal product), the CO_2 value from closest node (50.125°N, 4.125°W) in the Landschützer coastal product (Landschützer et al., 2020) is extrapolated across the study area. Fluxes were computed for a fixed region of 128 km^2 (a slight modification of the region in Figures 10b and 11a-d) encompassing the river plume and the region behind the Breakwater. Areas that met the depth and salinity criteria in the region (depth >10m, ξS > -4 and >50.24°N) for > 80% of the period were included. Whilst fCO_2 is typically measured weekly at L4 by the showerhead system, instrument downtime in 2016 meant that the measurements were less frequent than normal, leading to interpolation between measurements to construct a non-fragmented timeseries of seasonal fCO_2 in 2016 (an unavoidable limitation of this approach). The average regional fCO_2 (i.e. including using the spatially varying salinity) showed undersaturation in the summer and oversaturation in the spring and autumn. The regional concentration was ~30 µatm greater than the observed concentrations at L4, which is larger than the uncertainty in our estimate of fCO_2 (Figure 12). The pCO_2 in the Landschützer coastal product was much lower than the observed fCO_2 values at L4 in 2016 (Figure 12).

L4 *p*CO2 saturations (Figure 12) indicate that fluxes follow the same trend as previous measurements at the site: CO_2 uptake in the region throughout the summer and a short period of outgassing in late September (Kitidis et al., 2012;Marrec et al., 2013). The Landschützer product suggests that the region is a larger sink than indicated by the measurements at L4, and does not indicate that the region is ever a source of CO_2 to the atmosphere. This study calculates fluxes using fCO_2 values predicted from salinity and suggests that the near coastal region (128 km^2) was a weaker sink in summer, increasing the discrepancy with the Landschützer product. This study also suggests weak outgassing of CO_2 near the coast in March, April and October

5. Discussion

Here we show large variations in fCO_2 in the estuarine zone using a high-frequency membrane equilibrator which could not be detected using a showerhead equilibrator. Seawater fCO_2 is assumed to be relatively homogeneous over large spatial scales in the open ocean (Takahashi et al., 2009). Temporal variability in open ocean waters is also typically slow, with the most rapid variations occurring over hourly or slower timescales (e.g. diurnal (Torres et al., 2021)). The measuring frequency of a typical showerhead seawater CO_2 system (~8 min) is thus sufficient to determine open ocean fCO_2 variability. The difference between the underway fCO_2 measurements made by the two systems used in this study (Figure 2) is caused by the different response times of the showerhead and membrane equilibrators and their ability to resolve the considerable horizontal variability in coastal and shelf waters (Kitidis et al., 2012). The membrane and showerhead systems agreed well when the ship was on station (RMSE = 6.9 µatm), because both systems had sufficient time to equilibrate. When the ship was moving through heterogeneous coastal surface waters, the showerhead system cannot fully equilibrate, and the agreement with the fast-response membrane equilibrator system is worse (RMSE = 27.1 µatm).

Single seawater CO_2 observations are representative of CO_2 integrated across the region that the ship transits through whilst equilibrating. The RV *Plymouth Quest* typically travels at ~9 knots (4.6 m/s), which is equivalent to 0.22 km in 48 s (2 times the e-folding response time of the membrane system) and 1.1 km in 4 minutes (2 times the e-folding response time of the showerhead system). However, the showerhead system also switches between seawater CO_2, CO_2 gas standards and atmospheric CO_2, hence seawater measurements are not continuous. This routine means that seawater fCO_2 measurements are 27 min apart, which equates to a distance of ~7.5 km when the RV *Plymouth Quest* is moving.

We identified an inverse linear relationship between salinity and fCO_2 and that salinity measurements also agreed well with model salinity output. The FVCOM model output confirms that the river plume extent is highly variable in time and space, and that oceanographic features in the region such as the river plume are ~1 km or smaller. The highly dynamic nature of the plume means that a showerhead CO_2 system cannot be expected to resolve the spatial dynamics. A showerhead fCO_2 system design can also be biased toward the end of the equilibration period, which may generate some measurement bias if seawater fCO_2 changes rapidly during the 8 min full equilibration time (e.g. (Ribas-Ribas et al., 2014)). Complete characterisation of fCO_2 in coastal waters within 10 km of land and with highly variable fCO_2 requires a system with a fast response equilibrator or slower steaming.

Mixing of estuarine and continental shelf water masses partially determines the fCO_2 levels observed in this near shore study region. Shelf waters exhibit a seasonal surface fCO_2 trend associated with: a) cooling-enhanced solubility in late winter; b) net phytoplankton uptake in spring/summer; c) partial re-equilibration with the atmosphere; and d) mixing with CO_2-rich bottom waters in autumn (Kitidis et al., 2019). The River Tamar is the other mixing end member and is typically

oversaturated with fCO_2 with respect to the atmosphere (Frankignoulle et al., 1998). The results presented in this paper also suggest that riverine fCO_2 may have a strong influence on the spatial and temporal patterns in coastal waters off Plymouth. It is important to note that the relationship between salinity and fCO_2 determined in this paper only explains 21.6% of the variability, and was derived with summer data only (due to sampling constraints) Further work is needed to confirm if the relationship holds during the remaining period of the year (i.e. October through to May).

The fCO_2 variability that is not explained by our relationship could be driven by other factors. Close to the coast such as in Cawsand Bay, these include gas exchange in shallow waters, excess river runoff during storms, CO_2 production in sediments, upwelling of water with different CO_2 concentration, and biological activity stimulated by nutrients in the Tamar plume. Biological processes in coastal ecosystems can strongly influence seawater CO_2 levels (Cai et al., 2020),which may explain some of the large CO_2 changes observed around L4 that are not linked to salinity changes. fCO_2 changes due to photosynthesis are typically a few μatm per day (Kitidis et al., 2019) so large differences will likely have built up over time. Water masses with fCO_2 levels different to L4 may well be caused by factors such as biological activity, and then the water advected toward L4 by currents.

The confluence of estuarine and continental shelf waters near the PPAO/Breakwater and the local circulation of surface waters are dominated by the semi diurnal tidal cycle (Uncles et al., 2015). The rising tide after low water pushes shelf water toward the Breakwater, whereas a falling tide after high water encourages riverine-influenced water to extend south. The tidal influence upon coastal fCO_2 is evident in the 15 transects during this study, with changes of 20–40 μatm relative to L4 (Figure 8). Timeseries data presented by Borges and Frankignoulle (1999) indicate a similar magnitude (20–25 μatm) tidal signature in coastal Belgian and Dutch waters.

The salinity field from the FVCOM model is used to estimate the surface fCO_2 features over a complete tidal cycle and shows that the flux can change by a non-trivial amount (~9%) over a short period of time (Figure 11). These data also show that using a hydrodynamic model can extend the spatial and temporal coverage of CO_2 uptake and outgassing estimates in the coastal region surrounding Plymouth made with weekly L4 measurements (Figure 12). If similar relationships can be developed for other estuarine zones, then operational dynamic models may also be able to add information to flux estimates for these zones. The spatial resolution of the model at the surface means that it is possible that near surface features such as fresh water lenses are overlooked by this analysis. Higher resolution modelling of the surface ocean would make future coastal products more applicable to air/sea flux studies.

6. Conclusions

Here we show for the first time dynamic and large variations in the coastal zone using a fast response membrane equilibrator system. These gradients between estuarine waters and shelf waters were not resolved by a co-located showerhead CO_2 system. The gradients in salinity and fCO_2 fields show strong tidal influence. Changes in fCO_2 after accounting for the seasonal trend, are linked with salinity variations, with the highest regions of fCO_2 coinciding with the lowest salinity regions and vice versa. The inverse linear relationship between salinity and fCO_2 variations (Figure 8) suggests that mixing of estuarine and shelf water end members is a control on the surface water distribution of fCO_2. Measured salinity agrees well with FVCOM model surface salinity fields at different stages of the tidal cycle. FVCOM output is used to estimate the temporal and spatial variations of fCO_2 in coastal waters. The model output demonstrates that neglecting the river plume leads to an overestimation of the magnitude of the CO_2 sink in the summer. The region may also be misidentified as a sink for atmospheric CO_2 in the spring and autumn when it could be a weak source, as suggested by (Torres et al., 2020). Measurements from L4 are not representative of the estuarine zone and caution should be used when scaling them over this region.

The surface flux from estuaries and coastal waters has proven difficult to assess comprehensively (Borges et al., 2006). The high resolution fCO_2 data presented in this study show that tidal and estuarine-influenced coastal waters can quickly transition from a strong source to a strong sink depending on the state of the tide (Figure 11). Inland and coastal waters are a large uncertainty in global fluxes (Chen et al., 2013). The high resolution observations presented in this paper show that the head of the river/estuarine plume for this region is linked to the tidal state. This is critical for the accurate calculation of air–water flux from the region. Further studies are required to evaluate the wider applicability of this method to similar coastal regions. Distinctly different estuarine/coastal zones such as lagoons, river deltas and fjords will have their own distinct fCO_2 signatures and patterns driven in part by surface water circulation and mixing. High-resolution models that can resolve tides and surface salinity in estuarine/coastal waters with high confidence, are a useful tool in ongoing and future efforts to constrain coastal air–sea CO_2 fluxes.

7. Acknowledgements

This research was supported by UK NERC via studentship (NE/L000075/1), the Shelf Sea Biogeochemistry pelagic research programme (NE/K002007/1), RAGNARoCC (NE/K002473/1), single centre national capability (CLASS; NE/R015953/1), the Land Ocean Carbon Transfer project (LOCATE; NE/N018087/1), NERC grant NE/L007010 and the NERC LTSS National Capability Program that underpins numerical modelling work at PML. This research was also supported by EU projects MyCoast (EU Interreg Atlantic Area Program project MYCOAST (EAPA_285/2016)), IMMERSE (H2020 821926), AtlantOS (H2020 633211), FixO3 (FP7 312463) and RINGO (H2020 730944). We thank the captain and crew of

the RV *Plymouth Quest* for all their assistance. We also thank Tim Smyth and Ming Yang for insightful discussions and data relating to the WCO and PPAO time series and John Stevens and Rachel Beale for their help on the *PML Explorer*.

8. References

Abril, G., Bouillon, S., Darchambeau, F., Teodoru, C., Marwick, T., Tamooh, F., Ochieng Omengo, F., Geeraert, N., Deirmendjian, L., and Polsenaere, P.: Large overestimation of pCO 2 calculated from pH and alkalinity in acidic, organic-rich freshwaters, Biogeosciences, 12, 67-78, 2015.

Ahmed, M., and Else, B. G.: The Ocean CO2 Sink in the Canadian Arctic Archipelago: A Present-Day Budget and Past Trends Due to Climate Change, Geophysical research letters, 46, 9777-9785, 2019.

Bakker, D. C., de Baar, H. J., and de Wilde, H. P.: Dissolved carbon dioxide in Dutch coastal waters, Marine Chemistry, 55, 247-263, 1996.

Bakker, D. C., Pfeil, B., Landa, C. S., Metzl, N., O'brien, K. M., Olsen, A., Smith, K., Cosca, C., Harasawa, S., and Jones, S. D.: A multi-decade record of high-quality fCO 2 data in version 3 of the Surface Ocean CO 2 Atlas (SOCAT), Earth System Science Data, 8, 383, 2016.

Bauer, J. E., Cai, W.-J., Raymond, P. A., Bianchi, T. S., Hopkinson, C. S., and Regnier, P. A.: The changing carbon cycle of the coastal ocean, Nature, 504, 61, 2013.

Borges, A., and Frankignoulle, M.: Daily and seasonal variations of the partial pressure of CO 2 in surface seawater along Belgian and southern Dutch coastal areas, Journal of marine systems, 19, 251-266, 1999.

Borges, A., Schiettecatte, L.-S., Abril, G., Delille, B., and Gazeau, F.: Carbon dioxide in European coastal waters, Estuarine, Coastal and Shelf Science, 70, 375-387, 2006.

Borges, A. V., Abril, G., and Bouillon, S.: Carbon dynamics and CO 2 and CH 4 outgassing in the Mekong delta, Biogeosciences, 15, 1093-1114, 2018.

Bozec, Y., Cariou, T., Macé, E., Morin, P., Thuillier, D., and Vernet, M.: Seasonal dynamics of air-sea CO2 fluxes in the inner and outer Loire estuary (NW Europe), Estuarine, Coastal and Shelf Science, 100, 58-71, 2012.

Cai, W.-J.: Estuarine and coastal ocean carbon paradox: CO2 sinks or sites of terrestrial carbon incineration?, Annual Review of Marine Science, 3, 123-145, 2011.

Cai, W.-J., Xu, Y.-Y., Feely, R. A., Wanninkhof, R., Jönsson, B., Alin, S. R., Barbero, L., Cross, J. N., Azetsu-Scott, K., and Fassbender, A. J.: Controls on surface water carbonate chemistry along North American ocean margins, Nature communications, 11, 1-13, 2020.

Cai, W.-J., Feely, R. A., Testa, J. M., Li, M., Evans, W., Alin, S. R., Xu, Y.-Y., Pelletier, G., Ahmed, A., and Greeley, D. J.: Natural and anthropogenic drivers of acidification in large estuaries, Annual Review of Marine Science, 13, 23-55, 2021.

Cai, W., Chen, C. A., and Borges, A.: Carbon dioxide dynamics and fluxes in coastal waters influenced by river plumes, Biogeochemical Dynamics at Major River-Coastal Interfaces, edited by: Bianchi, TS, Allison MA, and Cai, W.-J., Cambridge University Press, Cambridge, 155-173, 2013.

Call, M., Maher, D. T., Santos, I. R., Ruiz-Halpern, S., Mangion, P., Sanders, C. J., Erler, D. V., Oakes, J. M., Rosentreter, J., and Murray, R.: Spatial and temporal variability of carbon dioxide and methane fluxes over semi-diurnal and spring–neap–spring timescales in a mangrove creek, Geochimica et Cosmochimica Acta, 150, 211-225, 2015.

Canning, A. R., Fietzek, P., Rehder, G., and Körtzinger, A.: Seamless gas measurements across the land–ocean aquatic continuum–corrections and evaluation of sensor data for CO 2, CH 4 and O 2 from field deployments in contrasting environments, Biogeosciences, 18, 1351-1373, 2021.

Cazenave, P. W., Torres, R., and Allen, J. I.: Unstructured grid modelling of offshore wind farm impacts on seasonally stratified shelf seas, Progress in Oceanography, 145, 25-41, 2016.

Chen, C.-T., Huang, T.-H., Chen, Y.-C., Bai, Y., He, X., and Kang, Y.: Air-sea exchanges of CO2 in the world's coastal seas, Biogeosciences, 10, 6509, 2013.

Chen, C.-T. A., and Borges, A. V.: Reconciling opposing views on carbon cycling in the coastal ocean: Continental shelves as sinks and near-shore ecosystems as sources of atmospheric CO2, Deep Sea Research Part II: Topical Studies in Oceanography, 56, 578-590, 2009.

Chen, C., Liu, H., and Beardsley, R. C.: An unstructured grid, finite-volume, three-dimensional, primitive equations ocean model: application to coastal ocean and estuaries, Journal of Atmospheric and Oceanic Technology, 20, 159-186, 2003.

Dai, M., Lu, Z., Zhai, W., Chen, B., Cao, Z., Zhou, K., Cai, W. J., and Chenc, C. T. A.: Diurnal variations of surface seawater pCO2 in contrasting coastal environments, Limnology and Oceanography, 54, 735-745, 2009.

Dickson, A. G., and Millero, F. J.: A comparison of the equilibrium constants for the dissociation of carbonic acid in seawater media, Deep Sea Research Part A. Oceanographic Research Papers, 34, 1733-1743, 1987.

Dickson, A. G.: Standard potential of the reaction: AgCl (s)+ 12H2 (g)= Ag (s)+ HCl (aq), and and the standard acidity constant of the ion HSO4− in synthetic sea water from 273.15 to 318.15 K, The Journal of Chemical Thermodynamics, 22, 113-127, 1990.

Dickson, A. G., Sabine, C. L., and Christian, J. R.: Guide to best practices for ocean CO_2 measurements, 2007.

Fennel, K., Alin, S., Barbero, L., Evans, W., Bourgeois, T., Cooley, S., Dunne, J., Feely, R. A., Hernandez-Ayon, J. M., and Hu, X.: Carbon cycling in the North American coastal ocean: a synthesis, Biogeosciences, 16, 1281-1304, 2019.

Ferrón, S., Ortega, T., Gómez-Parra, A., and Forja, J.: Seasonal study of dissolved CH4, CO2 and N2O in a shallow tidal system of the bay of Cádiz (SW Spain), Journal of marine systems, 66, 244-257, 2007.

Frankignoulle, M., Bourge, I., Canon, C., and Dauby, P.: Distribution of surface seawater partial CO 2 pressure in the English Channel and in the Southern Bight of the North Sea, Continental Shelf Research, 16, 381-395, 1996.

Frankignoulle, M., Abril, G., Borges, A., Bourge, I., Canon, C., Delille, B., Libert, E., and Théate, J.-M.: Carbon dioxide emission from European estuaries, Science, 282, 434-436, 1998.

Friedlingstein, P., Jones, M., O'Sullivan, M., Andrew, R., Hauck, J., Peters, G., Peters, W., Pongratz, J., Sitch, S., and Le Quéré, C.: Global carbon budget 2019, Earth System Science Data, 11, 1783-1838, 2019.

Hales, B., Chipman, D., and Takahashi, T.: High-frequency measurement of partial pressure and total concentration of carbon dioxide in seawater using microporous hydrophobic membrane contractors, Limnol. Oceanogr.: Methods 2, 356-364, 2004.

Hales, B., Takahashi, T., and Bandstra, L.: Atmospheric CO2 uptake by a coastal upwelling system, Global Biogeochemical Cycles, 19, 2005.

Haney, R. L.: On the pressure gradient force over steep topography in sigma coordinate ocean models, Journal of Physical Oceanography, 21, 610-619, 1991.

JCGM: Evaluation of measurement data—Guide to the expression of uncertainty in measurement, Int. Organ. Stand. Geneva ISBN, 50, 134, 2008.

Jeffrey, L. C., Maher, D. T., Santos, I. R., Call, M., Reading, M. J., Holloway, C., and Tait, D. R.: The spatial and temporal drivers of pCO2, pCH4 and gas transfer velocity within a subtropical estuary, Estuarine, Coastal and Shelf Science, 208, 83-95, 2018a.

Jeffrey, L. C., Santos, I. R., Tait, D. R., Makings, U., and Maher, D. T.: Seasonal drivers of carbon dioxide dynamics in a hydrologically modified subtropical tidal river and estuary (Caboolture River, Australia), Journal of Geophysical Research: Biogeosciences, 123, 1827-1849, 2018b.

Jiang, L. Q., Cai, W. J., Wanninkhof, R., Wang, Y., and Lüger, H.: Air-sea CO2 fluxes on the US South Atlantic Bight: Spatial and seasonal variability, Journal of Geophysical Research: Oceans, 113, 2008.

Joesoef, A., Huang, W.-J., Gao, Y., and Cai, W.-J.: Air–water fluxes and sources of carbon dioxide in the Delaware Estuary: spatial and seasonal variability, Biogeosciences, 12, 6085-6101, 2015.

Kahl, L. C., Bianchi, A. A., Osiroff, A. P., Pino, D. R., and Piola, A. R.: Distribution of sea-air CO2 fluxes in the Patagonian Sea: Seasonal, biological and thermal effects, Continental Shelf Research, 143, 18-28, 2017.

Kitidis, V., Hardman-Mountford, N. J., Litt, E., Brown, I., Cummings, D., Hartman, S., Hydes, D., Fishwick, J. R., Harris, C., and Martinez-Vicente, V.: Seasonal dynamics of the carbonate system in the Western English Channel, Continental Shelf Research, 42, 30-40, 2012.

Kitidis, V., Brown, I., Hardman-Mountford, N., and Lefèvre, N.: Surface ocean carbon dioxide during the Atlantic Meridional Transect (1995–2013); evidence of ocean acidification, Progress in Oceanography, 158, 65-75, 2017.

Kitidis, V., Shutler, J. D., Ashton, I., Warren, M., Brown, I., Findlay, H., Hartman, S. E., Sanders, R., Humphreys, M., and Kivimäe, C.: Winter weather controls net influx of atmospheric CO 2 on the north-west European shelf, Scientific Reports, 9, 1-11, 2019.

Körtzinger, A., Mintrop, L., Wallace, D. W., Johnson, K. M., Neill, C., Tilbrook, B., Towler, P., Inoue, H. Y., Ishii, M., and Shaffer, G.: The international at-sea intercomparison of fCO_2 systems during the R/V Meteor Cruise 36/1 in the North Atlantic Ocean, Marine Chemistry, 72, 171-192, 2000.

Landschützer, P., Laruelle, G. G., Roobaert, A., and Regnier, P.: A uniform pCO 2 climatology combining open and coastal oceans, Earth System Science Data, 12, 2537-2553, 2020.

Laruelle, G. G., Dürr, H. H., Slomp, C. P., and Borges, A. V.: Evaluation of sinks and sources of CO2 in the global coastal ocean using a spatially-explicit typology of estuaries and continental shelves, Geophysical research letters, 37, 2010.

Laruelle, G. G., Lauerwald, R., Pfeil, B., and Regnier, P.: Regionalized global budget of the CO2 exchange at the air-water interface in continental shelf seas, Global Biogeochemical Cycles, 28, 1199-1214, 2014.

Laruelle, G. G., Goossens, N., Arndt, S., Cai, W.-J., and Regnier, P.: Air–water CO 2 evasion from US East Coast estuaries, Biogeosciences, 14, 2441-2468, 2017a.

Laruelle, G. G., Landschützer, P., Gruber, N., Tison, J.-L., Delille, B., and Regnier, P.: Global high-resolution monthly pCO 2 climatology for the coastal ocean derived from neural network interpolation, Biogeosciences, 14, 4545-4561, 2017b.

Laruelle, G. G., Cai, W.-J., Hu, X., Gruber, N., Mackenzie, F. T., and Regnier, P.: Continental shelves as a variable but increasing global sink for atmospheric carbon dioxide, Nature communications, 9, 454, 2018.

Lefèvre, N., Diverrès, D., and Gallois, F.: Origin of CO2 undersaturation in the western tropical Atlantic, Tellus B: Chemical and Physical Meteorology, 62, 595-607, 2010.

Li, D., Chen, J., Ni, X., Wang, K., Zeng, D., Wang, B., Jin, H., Huang, D., and Cai, W. J.: Effects of Biological Production and Vertical Mixing on Sea Surface pCO2 Variations in the Changjiang River Plume During Early Autumn: A Buoy-Based Time Series Study, Journal of Geophysical Research: Oceans, 123, 6156-6173, 2018.

Litt, E. J., Hardman-Mountford, N. J., Blackford, J. C., Mitchelson-Jacob, G., Goodman, A., Moore, G. F., Cummings, D. G., and Butenschön, M.: Biological control of pCO2 at station L4 in the Western English Channel over 3 years, Journal of plankton research, 32, 621-629, 2010.

Macklin, P. A., Maher, D. T., and Santos, I. R.: Estuarine canal estate waters: Hotspots of CO2 outgassing driven by enhanced groundwater discharge?, Marine Chemistry, 167, 82-92, 2014.

Marrec, P., Cariou, T., Collin, E., Durand, A., Latimier, M., Macé, E., Morin, P., Raimund, S., Vernet, M., and Bozec, Y.: Seasonal and latitudinal variability of the CO2 system in the western English Channel based on Voluntary Observing Ship (VOS) measurements, Marine Chemistry, 155, 29-41, 2013.

Mehrbach, C.: Measurement of the apparent dissociation constants of carbonic acid in seawater at atmospheric pressure, 1973.

Mellor, G. L., and Yamada, T.: Development of a turbulence closure model for geophysical fluid problems, Reviews of Geophysics, 20, 851-875, 1982.

Najjar, R. G., Herrmann, M., Alexander, R., Boyer, E. W., Burdige, D. J., Butman, D., Cai, W., Canuel, E. A., Chen, R. F., and Friedrichs, M. A.: Carbon budget of tidal wetlands, estuaries, and shelf waters of Eastern North America, Global Biogeochemical Cycles, 32, 389-416, 2018.

Nightingale, P. D., Malin, G., Law, C. S., Watson, A. J., Liss, P. S., Liddicoat, M. I., Boutin, J., and Upstill-Goddard, R. C.: In situ evaluation of air-sea gas exchange parameterizations using novel conservative and volatile tracers, Global Biogeochemical Cycles, 14, 373-387, 2000.

Orr, H., Des Clers, S., Simpson, G., Hughes, M., Battarbee, R., Cooper, L., Dunbar, M., Evans, R., Hannaford, J., and Hannah, D.: Changing water temperatures: a surface water archive for England and Wales, 2010.

Rees, A. P., Gilbert, J. A., and Kelly-Gerreyn, B. A.: Nitrogen fixation in the western English Channel (NE Atlantic ocean), Marine Ecology Progress Series, 374, 7-12, 2009.

Resplandy, L., Keeling, R., Rödenbeck, C., Stephens, B., Khatiwala, S., Rodgers, K., Long, M., Bopp, L., and Tans, P.: Revision of global carbon fluxes based on a reassessment of oceanic and riverine carbon transport, Nature Geoscience, 11, 504-509, 2018.

Ribas-Ribas, M., Anfuso, E., Gómez-Parra, A., and Forja, J.: Tidal and seasonal carbon and nutrient dynamics of the Guadalquivir estuary and the Bay of Cádiz (SW Iberian Peninsula), Biogeosciences, 10, 4481-4491, 2013.

Ribas-Ribas, M., Rerolle, V., Bakker, D. C., Kitidis, V., Lee, G., Brown, I., Achterberg, E. P., Hardman-Mountford, N., and Tyrrell, T.: Intercomparison of carbonate chemistry measurements on a cruise in northwestern European shelf seas, Biogeosciences, 11, 4339-4355, 2014.

Robbins, L., Daly, K., Barbero, L., Wanninkhof, R., He, R., Zong, H., Lisle, J., Cai, W. J., and Smith, C.: Spatial and temporal variability of pCO2, carbon fluxes, and saturation state on the West Florida Shelf, Journal of Geophysical Research: Oceans, 123, 6174-6188, 2018.

Roobaert, A., Laruelle, G. G., Landschützer, P., Gruber, N., Chou, L., and Regnier, P.: The spatiotemporal dynamics of the sources and sinks of CO2 in the global coastal ocean, Global Biogeochemical Cycles, 33, 1693-1714, 2019.

Santos, I. R., Maher, D. T., and Eyre, B. D.: Coupling automated radon and carbon dioxide measurements in coastal waters, Environmental science & technology, 46, 7685-7691, 2012.

Shen, C., Testa, J. M., Li, M., Cai, W. J., Waldbusser, G. G., Ni, W., Kemp, W. M., Cornwell, J., Chen, B., and Brodeur, J.: Controls on carbonate system dynamics in a coastal plain estuary: A modeling study, Journal of Geophysical Research: Biogeosciences, 124, 61-78, 2019.

Siddorn, J., Allen, J., and Uncles, R.: Heat, salt and tracer transport in the Plymouth Sound coastal region: a 3-D modelling study, Journal of the Marine Biological Association of the United Kingdom, 83, 673-682, 2003.

Sims, R. P., Schuster, U., Watson, A. J., Yang, M. X., Hopkins, F. E., Stephens, J., and Bell, T. G.: A measurement system for vertical seawater profiles close to the air–sea interface, Ocean Science, 13, 649, 2017.

Skamarock, W. C., Klemp, J. B., Dudhia, J., Gill, D. O., Barker, D. M., Wang, W., and Powers, J. G.: A description of the Advanced Research WRF version 3. NCAR Technical note-475+ STR, 2008.

Smagorinsky, J.: General circulation experiments with the primitive equations: I. The basic experiment, Monthly weather review, 91, 99-164, 1963.

Smyth, T., Fishwick, J., Gallienne, C., Stephens, J., and Bale, A.: Technology, design, and operation of an autonomous buoy system in the western English Channel, Journal of Atmospheric and Oceanic Technology, 27, 2056-2064, 2010a.

Smyth, T. J., Fishwick, J. R., Lisa, A.-M., Cummings, D. G., Harris, C., Kitidis, V., Rees, A., Martinez-Vicente, V., and Woodward, E. M.: A broad spatio-temporal view of the Western English Channel observatory, Journal of Plankton Research, 32, 585-601, 2010b.

Takahashi, T., Sutherland, S. C., Wanninkhof, R., Sweeney, C., Feely, R. A., Chipman, D. W., Hales, B., Friederich, G., Chavez, F., and Sabine, C.: Climatological mean and decadal change in surface ocean pCO2, and net sea–air CO2 flux over the global oceans, Deep Sea Research Part II: Topical Studies in Oceanography, 56, 554-577, 2009.

Torres, O., Kwiatkowski, L., Sutton, A. J., Dorey, N., and Orr, J. C.: Characterizing mean and extreme diurnal variability of ocean CO2 system variables across marine environments, Geophysical research letters, 48, e2020GL090228, 2021.

Torres, R., Artioli, Y., Kitidis, V., Ciavatta, S., Ruiz-Villarreal, M., Shutler, J., Polimene, L., Martinez, V., Widdicombe, C., and Woodward, E. M. S.: Sensitivity of modeled CO2 air–sea flux in a coastal environment to surface temperature gradients, surfactants, and satellite data assimilation, Remote Sensing, 12, 2038, 2020.

Uncles, R., and Torres, R.: Estimating dispersion and flushing time-scales in a coastal zone: Application to the Plymouth area, Ocean & coastal management, 72, 3-12, 2013.

Uncles, R., Stephens, J., and Harris, C.: Estuaries of Southwest England: Salinity, suspended particulate matter, loss-on-ignition and morphology, Progress in Oceanography, 137, 385-408, 2015.

Uncles, R., Clark, J., Bedington, M., and Torres, R.: On sediment dispersal in the Whitsand Bay Marine Conservation Zone: neighbour to a closed dredge-spoil disposal site, in: Marine Protected Areas, Elsevier, 599-629, 2020.

Upstill-Goddard, R. C.: Air–sea gas exchange in the coastal zone, Estuarine, Coastal and Shelf Science, 70, 388-404, 2006.

Van Heuven, S., Pierrot, D., Rae, J., Lewis, E., and Wallace, D.: MATLAB Program Developed for CO2 System Calculations. ORNL/CDIAC-105b. Carbon Dioxide Information Analysis Center, Oak Ridge National Laboratory, US Department of Energy, Oak Ridge, Tennessee, cdiac. ornl. gov/ftp/co2sys/CO2SYS_calc_MATLAB_v1, 1, l, 2011.

Volta, C., Laruelle, G. G., and Regnier, P.: Regional carbon and CO2 budgets of North Sea tidal estuaries, Estuarine, Coastal and Shelf Science, 176, 76-90, 2016.

Wanninkhof, R.: Relationship between wind speed and gas exchange over the ocean revisited, Limnol. Oceanogr. Methods, 12, 351-362, 2014a.

Wanninkhof, R.: Relationship between wind speed and gas exchange over the ocean revisited, Limnology and Oceanography: Methods, 12, 351-362, 2014b.

Ward, N. D., Bianchi, T. S., Medeiros, P. M., Seidel, M., Richey, J. E., Keil, R. G., and Sawakuchi, H. O.: Where carbon goes when water flows: carbon cycling across the aquatic continuum, Frontiers in Marine Science, 4, 7, 2017.

Weiss, R. F.: Carbon dioxide in water and seawater: the solubility of a non-ideal gas, Marine chemistry, 2, 203-215, http://dx.doi.org/10.1016/0304-4203(74)90015-2, 1974.
Widdicombe, C., Eloire, D., Harbour, D., Harris, R., and Somerfield, P.: Long-term phytoplankton community dynamics in the Western English Channel, Journal of Plankton Research, 32, 643-655, 2010.
Woolf, D. K., Shutler, J. D., Goddijn-Murphy, L., Watson, A., Chapron, B., Nightingale, P. D., Donlon, C. J., Piskozub, J., Yelland, M., and Ashton, I.: Key uncertainties in the recent air-sea flux of CO2, Global Biogeochemical Cycles, 33, 1548-1563, 2019.
Yang, M., Bell, T. G., Hopkins, F. E., Kitidis, V., Cazenave, P. W., Nightingale, P. D., Yelland, M. J., Pascal, R. W., Prytherch, J., and Brooks, I. M.: Air–sea fluxes of CO2 and CH4 from the Penlee Point Atmospheric Observatory on the south-west coast of the UK, Atmospheric Chemistry and Physics, 16, 5745-5761, 2016.
Yang, M., Bell, T. G., Brown, I. J., Fishwick, J., Kitidis, V., Nightingale, P. D., Rees, A. P., and Smyth, T. J.: Insights from year-long measurements of air–water CH4 and CO2 exchange in a coastal environment, Biogeosciences, 16, 961-978, 2019.

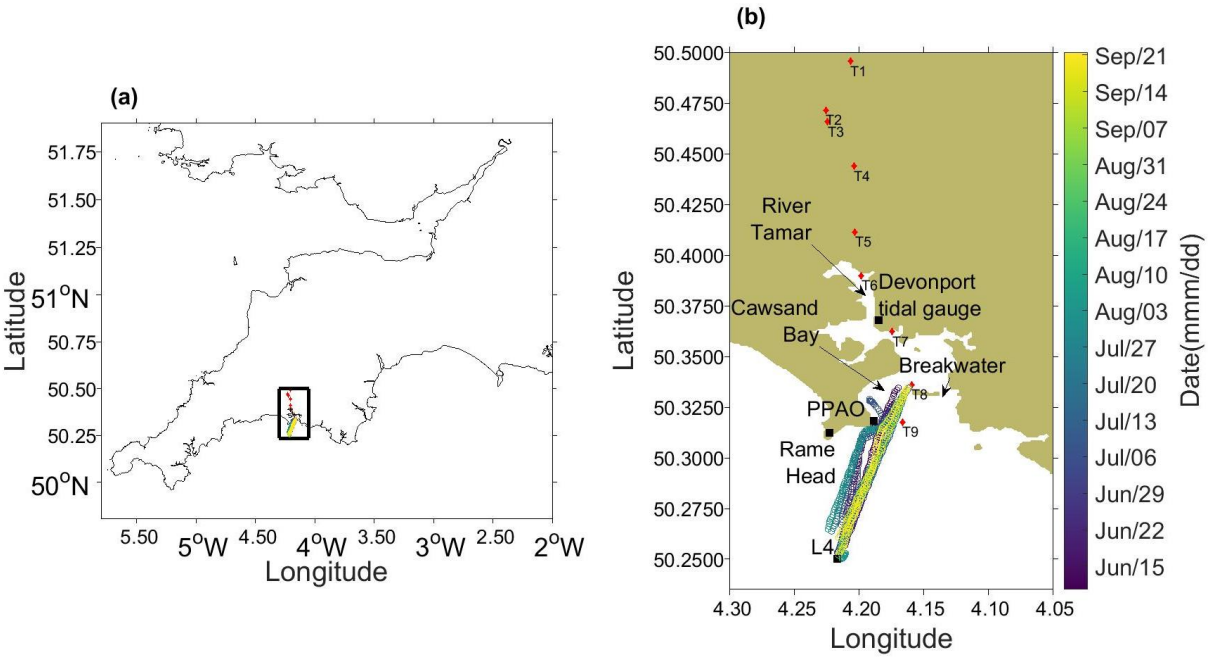

Figure 1: (a) Map of the Southwest of the England Western Channel Observatory (WCO) and study area (black rectangle). (b) Breakwater to L4 transects for the 15 transects made with the RV *Plymouth Quest* (coloured circles). Ship tracks are coloured by date between 10th June and 21st September 2016. The River Tamar, Devonport tidal gauge station, Plymouth Breakwater, Cawsand Bay, PPAO, Rame Head and Station L4 are marked. Transect sites T1–T9 are shown as red diamonds.

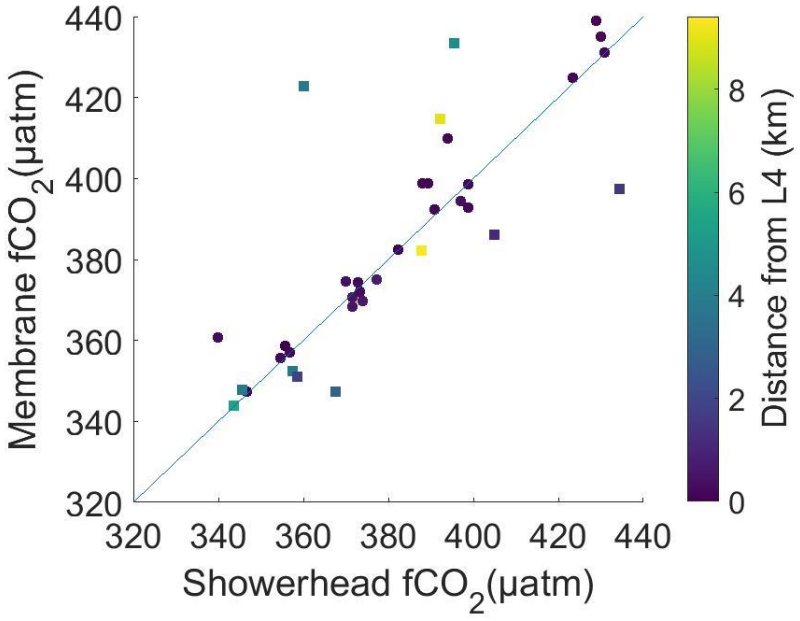

Figure 2: Comparison of coincident seawater fCO_2 measurements made using membrane and showerhead equilibrator systems on the RV *Plymouth Quest*. Both systems sampled from the underway seawater supply during transects between L4 and the Plymouth Breakwater (filled squares). The ship was stationary for long periods (>1 hour) at L4 (filled circles). The membrane equilibrator system was switched at L4 to tubing connected to a near surface profiler (Sims et al., 2017) while the showerhead system continued to sample from the underway supply. Data points are coloured as a function of distance from L4 (km). The 1:1 line represents perfect agreement and is shown for reference.

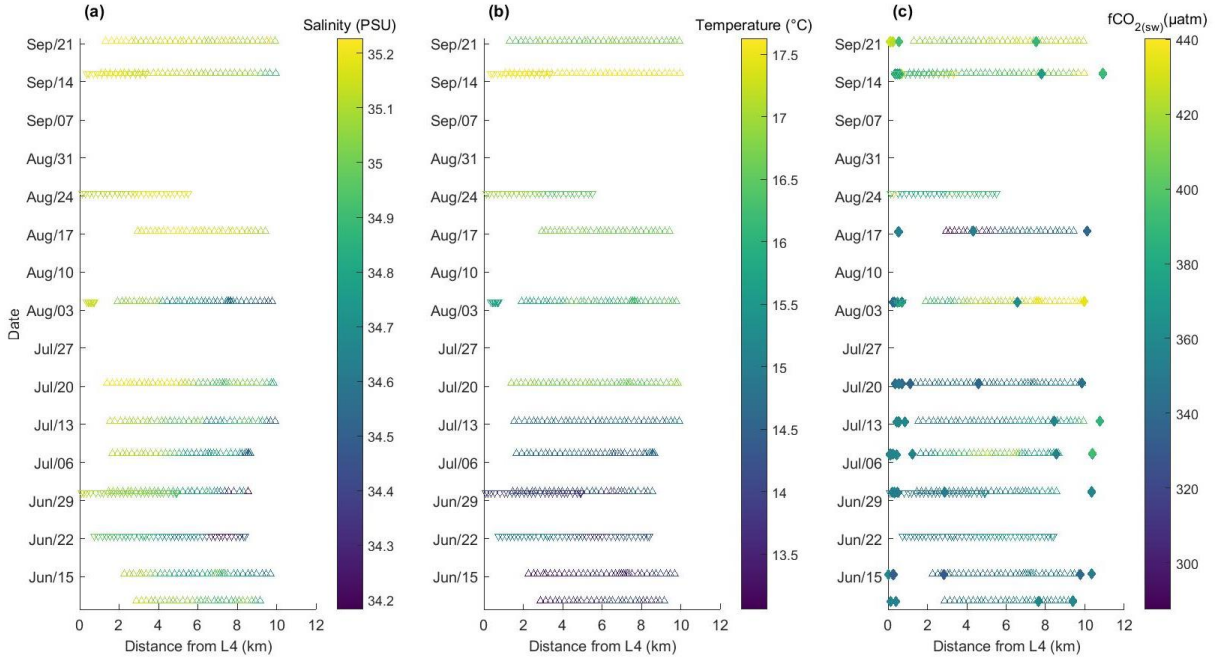

Figure 3: Surface water transects by RV *Plymouth Quest* between Plymouth Breakwater and station L4 from 10th June to 21st September 2016. Plotted are (a) salinity, (b) temperature and (c) fCO_2 as a function of distance from L4. Outbound transects are shown as downwards triangles and inbound transects are shown as upwards triangles for salinity, temperature and membrane equilibrator fCO_2 (sampling period = 0.5 min). Showerhead equilibrator fCO_2 observations are denoted by filled diamonds.

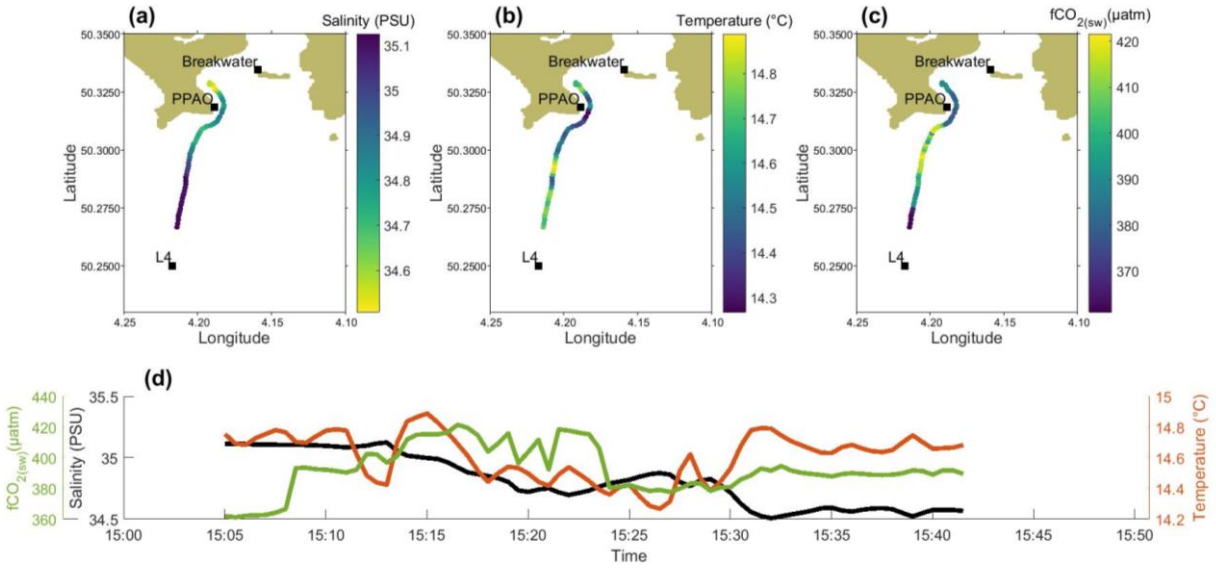

Figure 4: Example of a low water transect (transect mid-point = LW+0.5 hrs). Surface measurements of salinity, temperature and fCO_2 represented spatially (a to c) and as a time series (d) from station L4 toward the coast. Data were collected onboard RV Plymouth Quest on 7th July 2016 (filled circles, data every 30 sec).

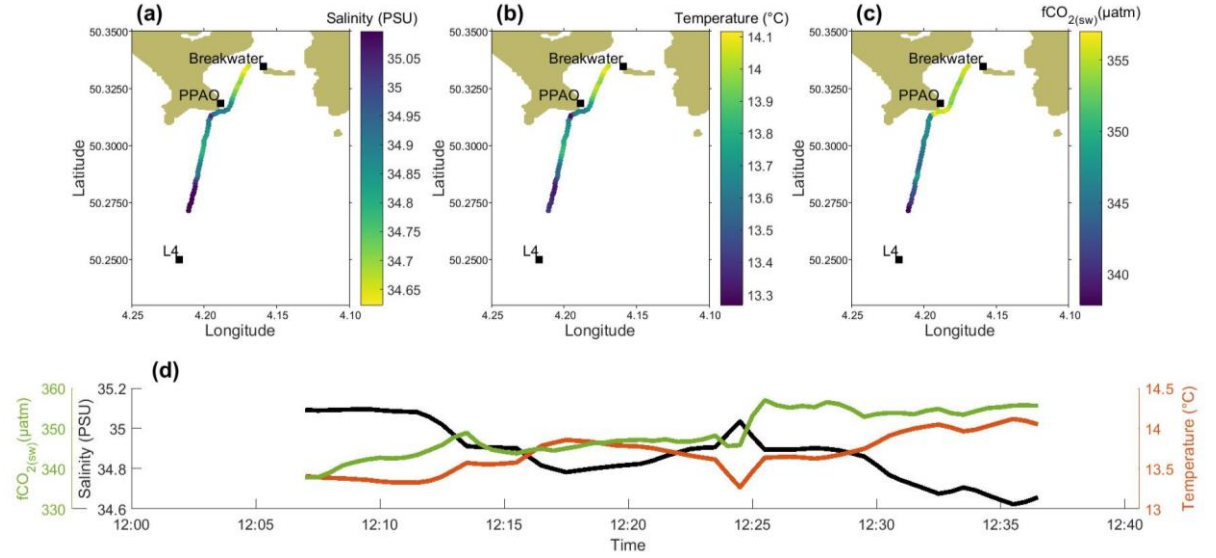

Figure 5: Example of a flooding tide transect (transect mid-point = LW+3.5 hrs). Surface measurements of salinity, temperature and fCO_2 represented spatially (a to c) and as a time series (d) from station L4 toward the coast. Data were collected onboard RV Plymouth Quest on 15th June 2016, (filled circles, data every 30 sec).

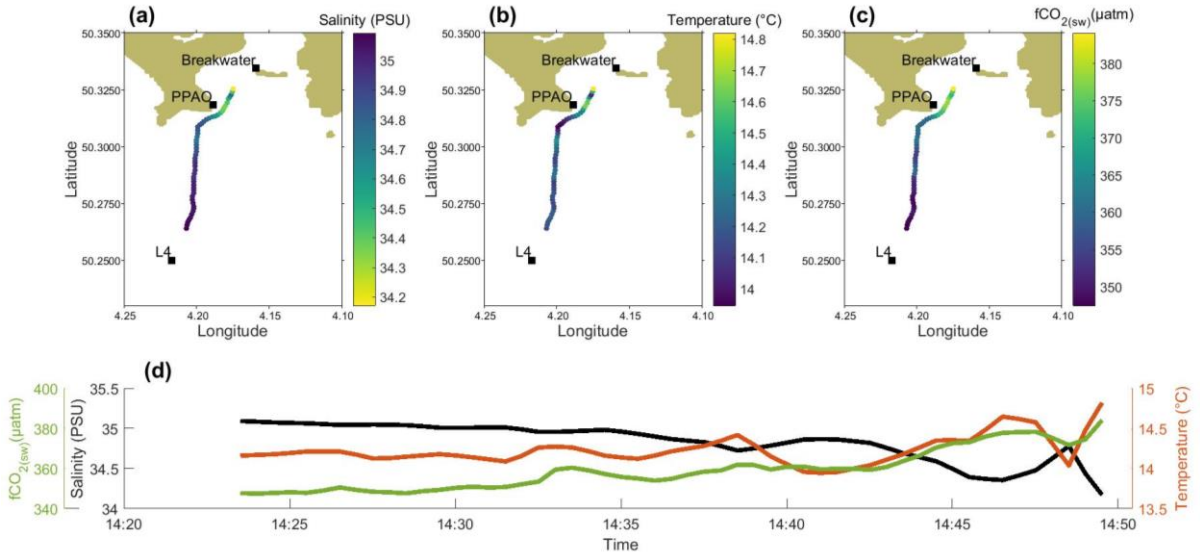

Figure 6: Example of a high water transect (transect mid-point = LW+6 hrs). Surface measurements of salinity, temperature and fCO_2 represented spatially (a–c) and as a time series (d) from station L4 toward the coast. Data were collected onboard RV Plymouth Quest on 30th June 2016, (filled circles, data every 30 sec).

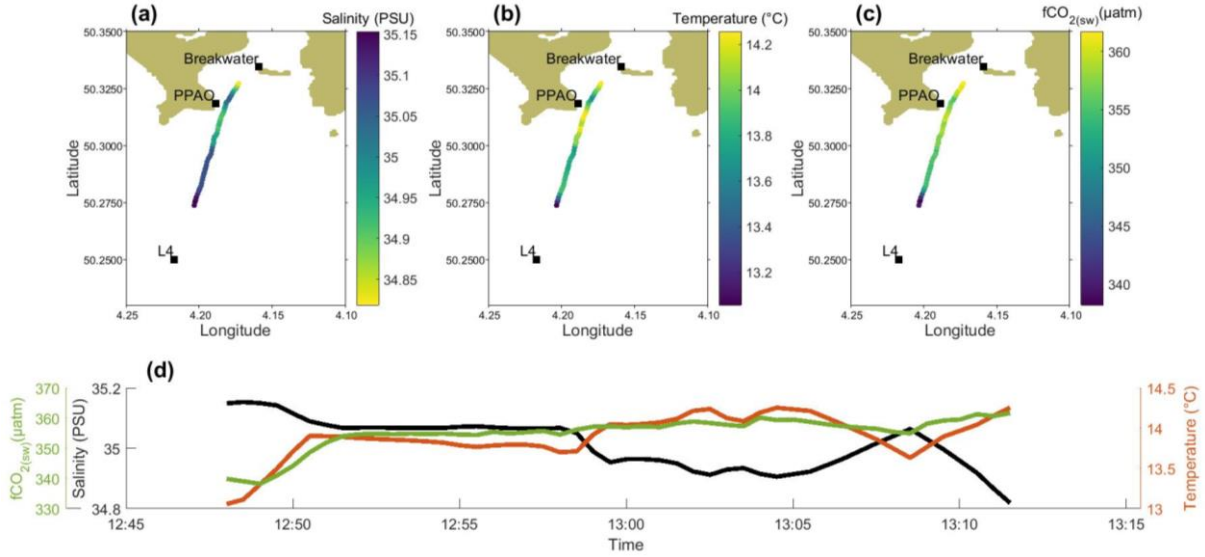

Figure 7: Example of an ebbing tide transect (transect mid-point = LW+8.75 hrs). Surface measurements of salinity, temperature and fCO_2 represented spatially (a–c) and as a time series (d) from station L4 toward the coast. Data were collected onboard RV Plymouth Quest on 10th June 2016, (filled circles, data every 30 sec).

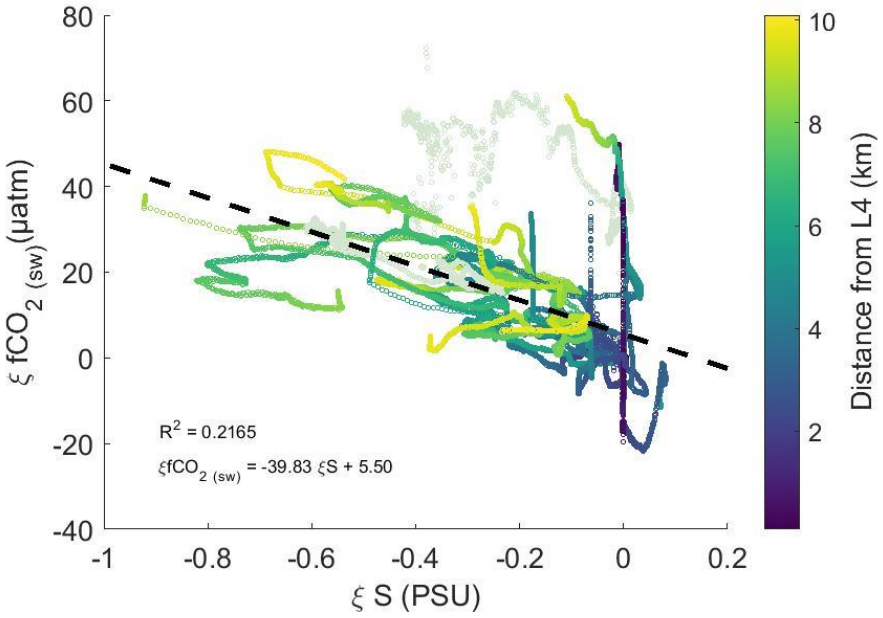

Figure 8: Scatter plot of ξS versus ξfCO$_2$, difference of data from transects between Plymouth Breakwater and station L4 between 10th June and 21st September 2016. Data are coloured by their distance from station L4, the dashed black line is the best fit for the data. The data for 7th July is shown in light grey.

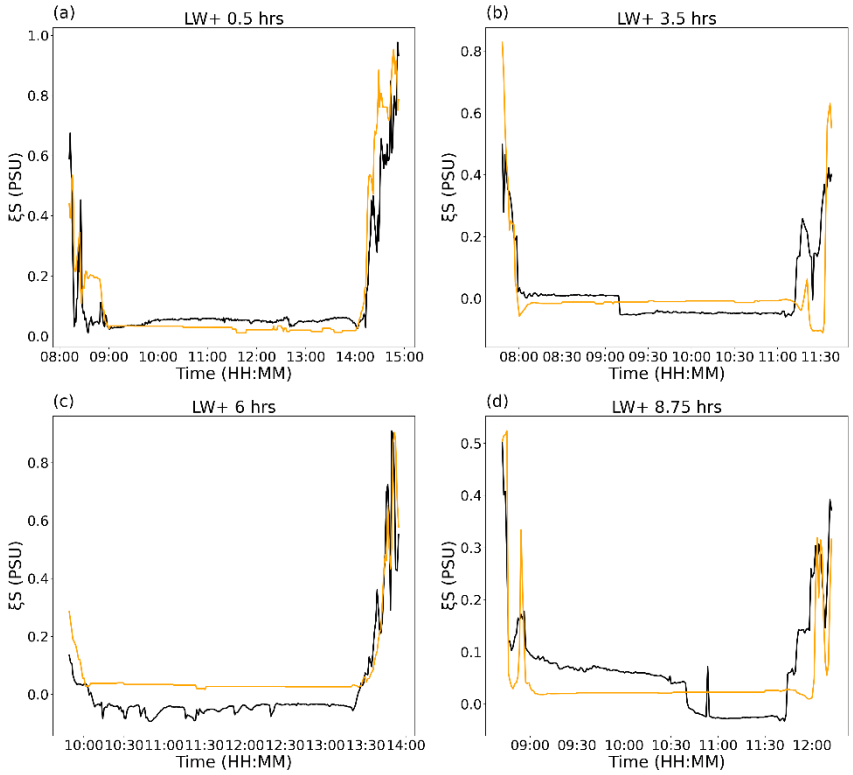

710

Figure 9: Comparison of ξS from surface observations (underway RV Plymouth Quest, black) and the FVCOM model (orange). Each of the four panels corresponds to the four example transects from four stages of the tidal cycle: (a) 7th July (LW+0hrs); (b) 15th June (LW+3.5hrs); (c) 30th June (LW+6hrs); and (d) 10th June (LW+8.75hrs).

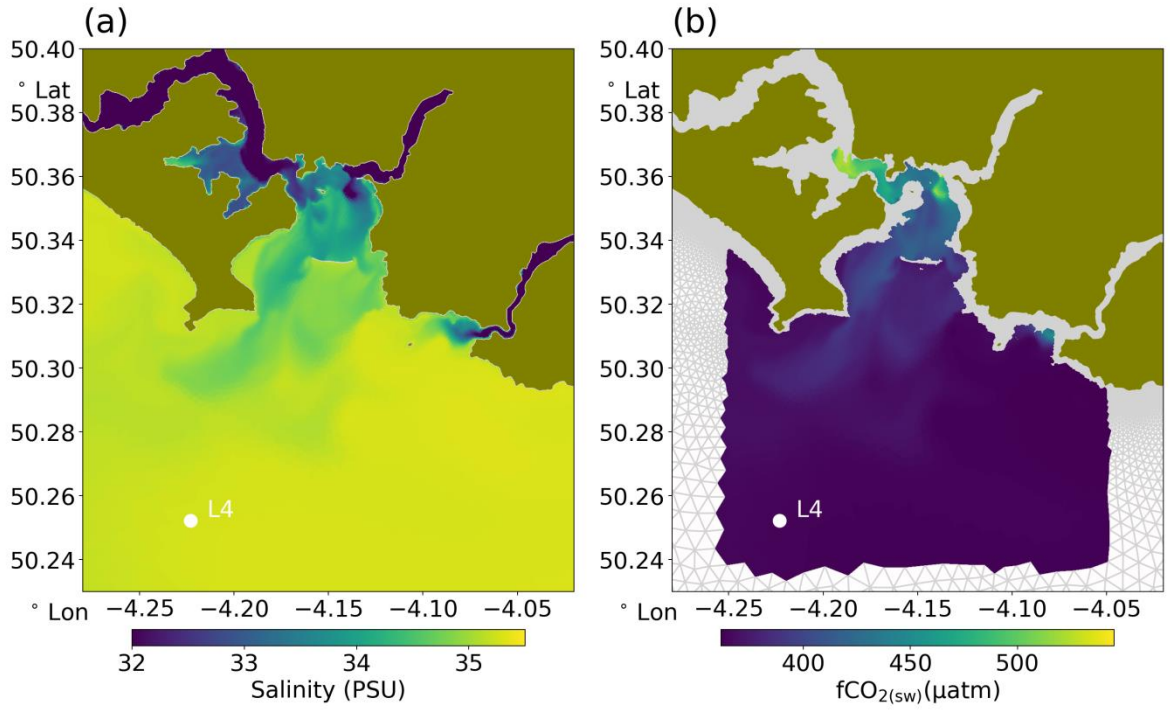

715 **Figure 10: (a) Model surface salinity field on 7th July at the midpoint of the observational transect. Note that the range of the colourbar was restricted to better depict salinity in the lower estuary and thus salinity in the upper estuaries is beyond the range of the colourbar. (b) derived ξfCO_2 using determined ξS and ξfCO_2 relationship.**

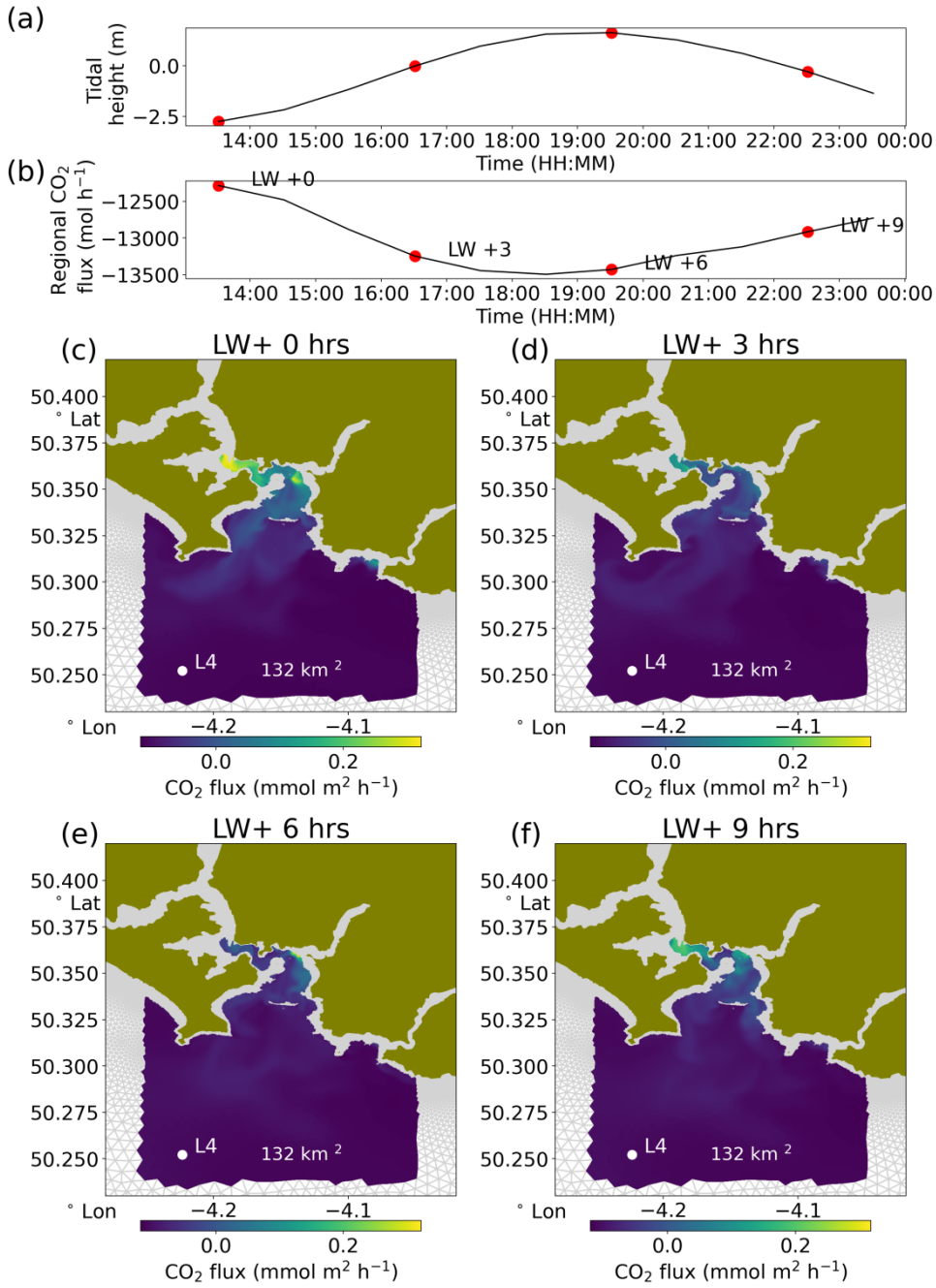

Figure 11: Modelled impact of a full tidal cycle (a) on tidal height (b) on air–sea CO_2 flux in the coastal zone (hourly calculations, negative fluxes are into the ocean) on 7th July 2016 with a fixed wind speed of 5.3ms^{-1}. The total integrated air–sea CO_2 flux within the modelled domain (c–f). Spatial variation in flux at four different stages of the 12 hour tidal cycle is shown: LW+0 hr (c). LW+3 hr (d), LW+6 hr (e). LW+9 hr (f). The red dots in (a) and (b) correspond to panels c–f.

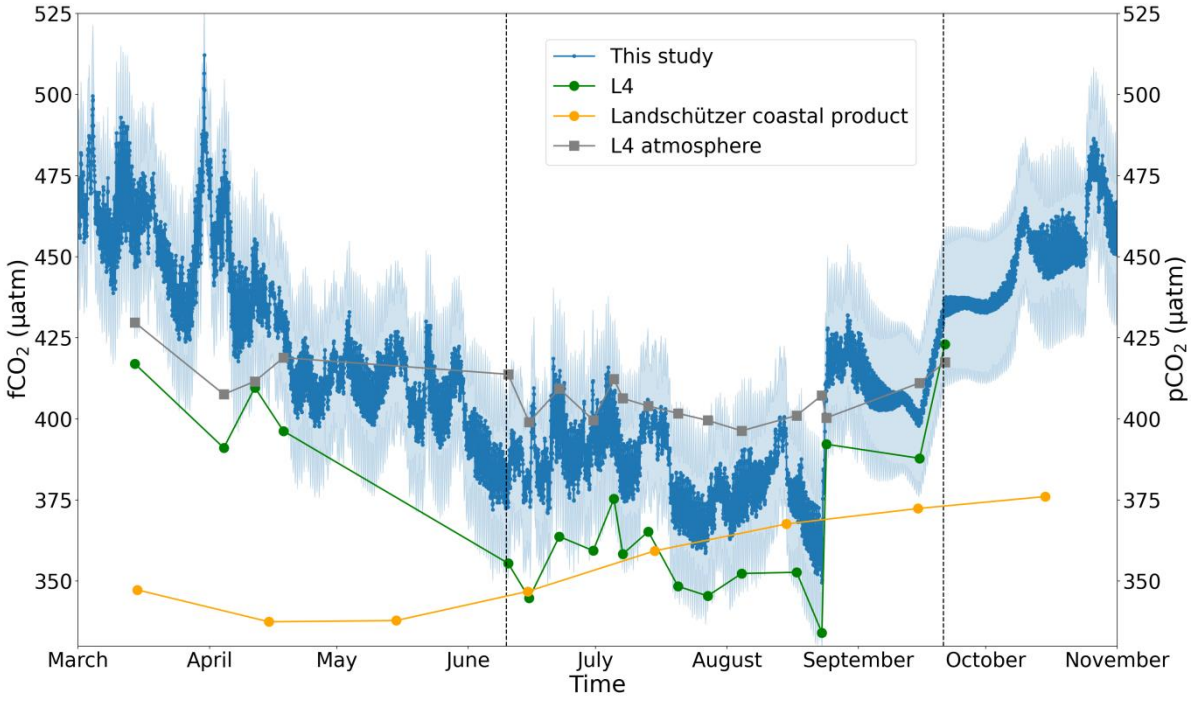

Figure 12: fCO_2 and pCO_2 values used to calculate regional CO_2 flux over the domain (128 km^2, approximately same as in above figures). Measurements of fCO_2 made by RV *Plymouth Quest* on station at L4 (L4, green dots). $pCO_{2\,(atm)}$ measured by Plymouth *Quest* on station at L4 (grey squares). The results of this study, hourly average fCO_2 across the valid model domain used for long term flux calculations (this study, blue dots). The standard combined uncertainty in the data from this study is indicated by the shaded background in light blue. The monthly Landschützer pCO_2 data (Landschützer coastal product, orange dots) is from the closest valid node (50.125°N, 4.125°W) in the Landschützer et al. (2020) coastal data product. It is noted that the Landschützer node is outside of the model domain (which has a lower boundary of 50.24°N).The vertical dashed lines indicate the dates of the first and last measurement transects.